Recent observations of tornadoes using a mobile, rapid-scan, polarimetric, X-band, Doppler radar

Howard B. Bluestein[1], Jeffrey C. Snyder[2], Kyle J. Thiem[1], Zachary B. Wienhoff[1], Jana B. Houser[3], and Vivek Mahale[1]

[1]*School of Meteorology, University of Oklahoma, Norman, Oklahoma 73072, U. S. A.*
[2]*National Severe Storms Laboratory, Norman, Oklahoma 73072, U. S. A.*
[3]*Department of Geography, Ohio University, Athens, Ohio 45701, U. S. A.*

(Dated: 15 July 2014)

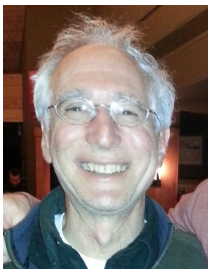

Howard (Howie "Cb") Bluestein

1 Introduction

Since the spring of 2011, a group at the University of Oklahoma in Norman has been using a mobile, rapid-scan, polarimetric, Doppler radar, RaXPol (Fig. 1), to study tornadogenesis and tornado structure (Pazmany et al. 2013), among

Figure 1: Photograph of RaXPol scanning a supercell in southwestern Oklahoma on 29 May 2013, just before a tornado (See Figs. 10 and 11 for other related figures) formed. View to the northeast. (photo © H. Bluestein)

Figure 2: Wide-angle photograph (© H. Bluestein) of a tornadic supercell southwest of Carney, Oklahoma on 19 May 2013. Arrow points to the condensation funnel of the tornado. A tail cloud is seen to the right.

hblue@ou.edu

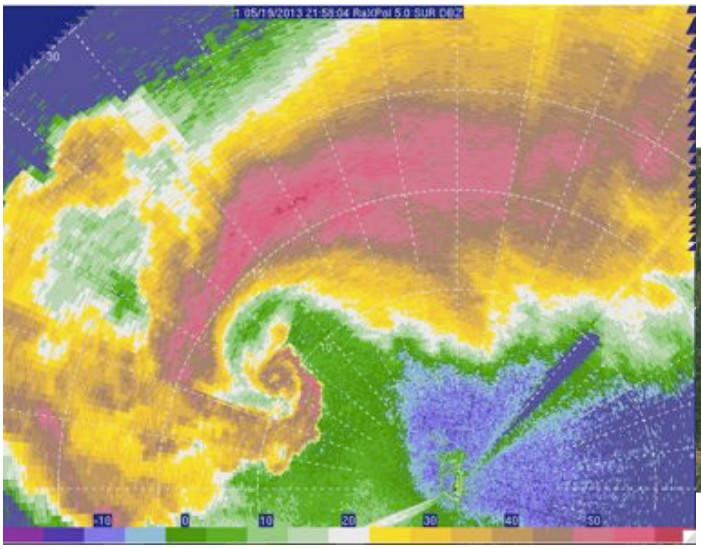

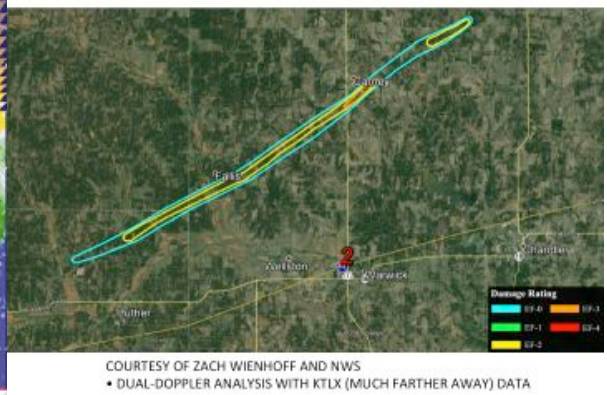

Figure 3 (above left): Radar reflectivity factor Z (dBZ) from RaXPol, at 5^0 elevation angle, at 2158:04 UTC 19 May 2013, of the Edmond – Carney, Oklahoma tornadic supercell. A weak-echo hole (WEH) marks the center of the tornado, at the tip of the hook echo. Range rings shown every 5 km.

Figure 4 (above right): Damage track of the Edmond – Carney tornado and the second ("2") deployment location of RaXPol.

Figure 5: Frame grab of a video (© H. Bluestein) of the multiple-vortex stage of the Norman – Shawnee tornado, just northeast of Norman, Oklahoma on 19 May 2013. View is to the southwest from deployment location 3 (see Fig. 7 below).

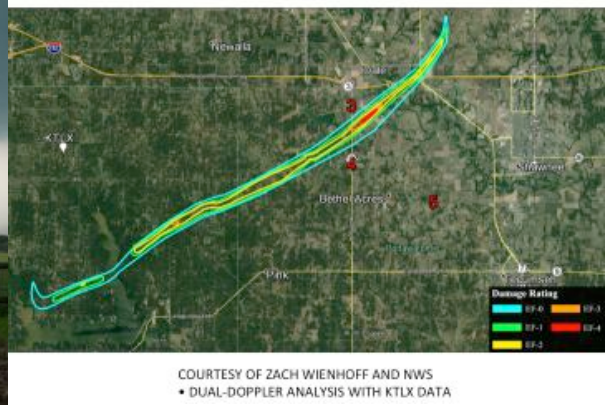

Figure 6 (above left): Single-vortex stage of the Norman – Shawnee tornado and a tail cloud, zoomed out view, on 19 May 2013, as seen from deployment location 3 (see Fig. 7).

Figure 7 (above right): As in Fig. 4, but deployment locations 3, 4, and 5 for the Norman – Shawnee tornado.

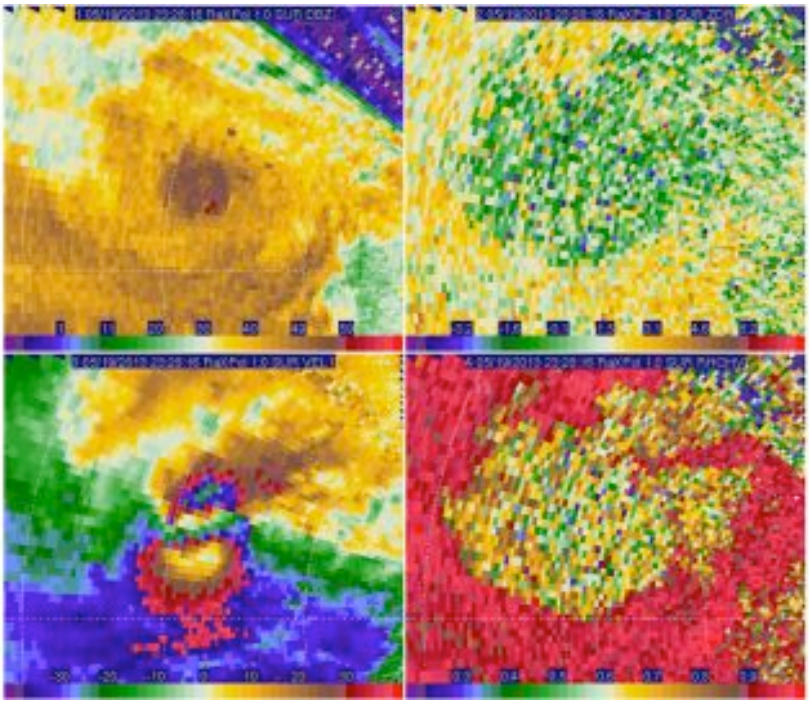

Figure 8: RaXPol data at 2328:16 UTC 19 May 2013, at 1^0 elevation angle, from deployment location 4 (see Fig. 7), for the Norman – Shawnee tornado. Range rings plotted every 1 km. (top left) radar reflectivity factor Z (dBZ); (top right) differential reflectivity Z_{DR} (dB); (bottom left) aliased Doppler velocity V (m s^{-1}); (bottom right) co-polar correlation coefficient ρ_{hv}. There is no weak-echo hole (WEH), but the debris signature is well defined in both Z_{DR} and ρ_{hv}, surrounding the cyclonic-shear vortex signature.

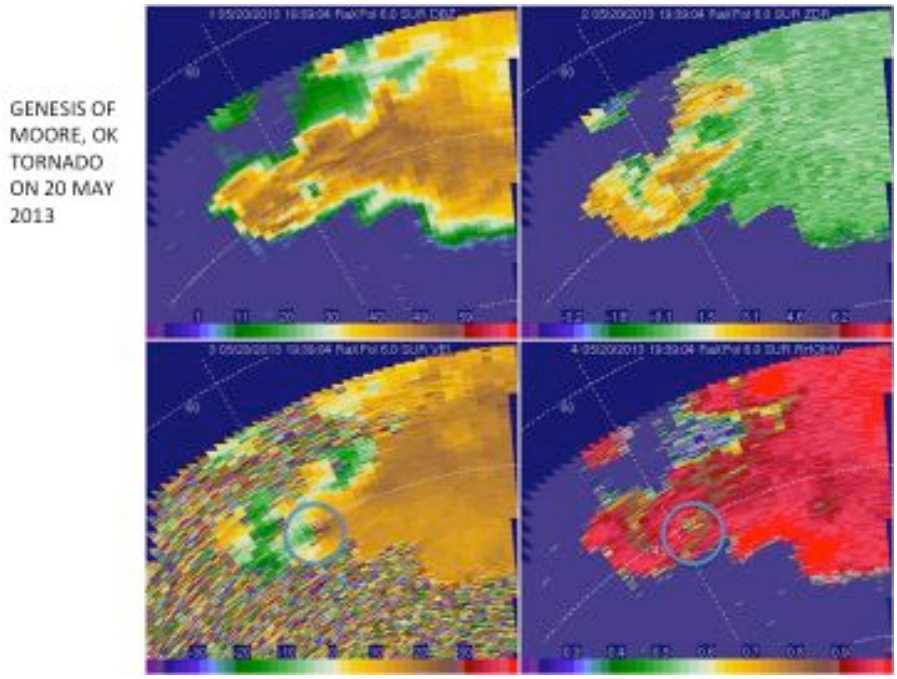

Figure 9: As in Fig. 8, but for the Moore, Oklahoma tornado on 20 May 2013. Range rings shown every 15 km. The circles enclose the vortex cyclonic-shear couplet and the debris signature. A weak-echo hole (WEH) is seen in reflectivity.

other things. This radar scans mechanically very rapidly by making use of frequency hopping to increase the number of samples so that high accuracy can be achieved. In most cases the data were oversampled, while the radial resolution varied from 75 m down to 15 m. The purpose of this extended abstract is to show a sample of the most significant datasets collected in 2013 that document tornadogenesis and tornado structure. Data from a few of these datasets have already been used to compare independent, EF-scale ratings of damage with the radar observations and to improve estimates of Doppler velocity in tornado debris clouds (Snyder and Bluestein 2014). The datasets are unique in that they document Doppler velocity and polarimetric variables at each elevation angle every 2 s, which is extremely rapid.

2 Cases

Figs. 1 – 8 illustrate data collection in a tornadic supercell that tracked from Edmond to Carney, OK (in central Oklahoma) and in a second, nearby, tornadic supercell that tracked from Norman to Shawnee, OK. Fig. 2 shows the Edmond-Carney tornado during data collection. Fig. 3 shows the low-altitude radar reflectivity field of this storm while the tornado was in progress. Fig. 4 shows the location of RaXPol in relation to the damage path of the first tornado. Fig. 5 shows the multiple-vortex stage of the second, Norman – Shawnee tornado during data collection (Fig. 7). Fig. 6 shows the single-vortex stage of the tornado in relation to other storm features. Fig. 8 shows polarimetric Doppler data from the Norman – Shawnee tornado at low altitude when it was very close (~ 2 - 3 km range) to the radar. The debris signature shows up clearly in both Z_{DR} and ρ_{hv}. Zach Wienhoff is analyzing both volumetric datasets in detail, including dual-Doppler analysis using WSR-88D data from nearby KTLX and data from RaXPol. Both datasets cover the evolution of the tornadoes beginning ~ 2 min after tornadogenesis and the latter is of high-enough resolution, when the radar was at deployment site 4, to document some aspects of tornado structure above the surface friction layer.

The beginning of the large tornadic supercell that struck Newcastle and Moore, Oklahoma on 20 May 2013 was probed by RaXPol (Fig. 9). Unfortunately, the crew had targeted an area to the south and southwest, so it was not possible to collect close-up, high-resolution data. Nevertheless, a vortex signature and tornado-debris signature were resolved, but data were not collected for a long-enough period of time to document tornadogenesis or tornado evolution.

Figure 10: Photograph of large hail (© H. Bluestein) that fell in southwestern Oklahoma at a deployment site just before tornadogenesis, while RaXPol was collecting data on 29 May 2013.

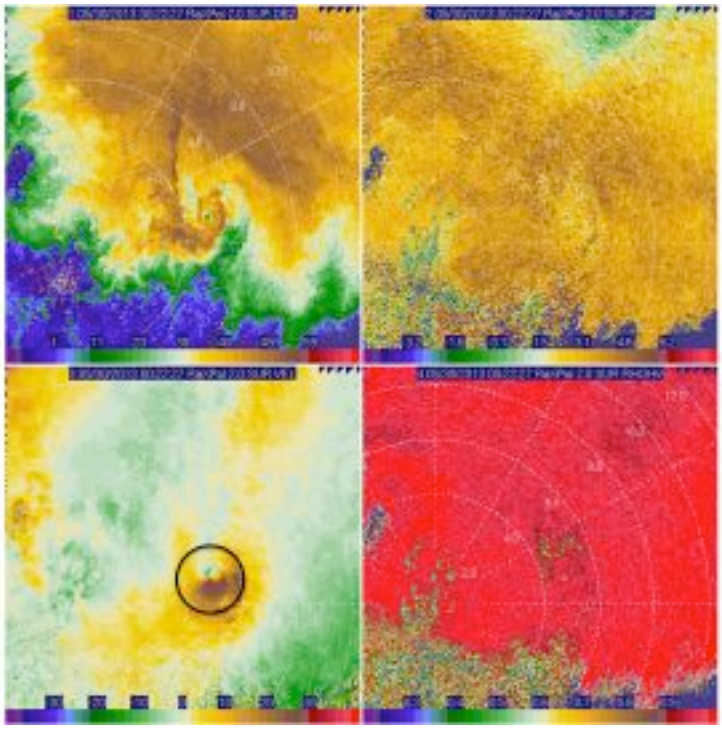

Figure 11: Like Fig. 8, but at 2^0 elevation angle, at 0022:27 UTC 30 May 2013. Range rings plotted every 2 km. Circle encloses cyclonic vortex signature associated with tornado.

On 29 May 2013, while being hit with ellipsoidally shaped hail as large as 3 inches along its major axis (Fig. 10), volumetric data were collected (Fig. 1) as a small, weak tornado formed (Fig. 11).

On 30 May 2013 data were collected in a supercell that did not produce a tornado; however, during data collection, a funnel cloud was noted in a supercell just to the west of the targeted storm (Fig. 12) while data were being collected (Fig. 13).

Figure 12: Composite photographs (© H. Bluestein) of a cyclonically rotating wall cloud and tail cloud in south-central Oklahoma on 30 May 2013, and a funnel cloud (arrow) in a storm to the west. View is to the north.

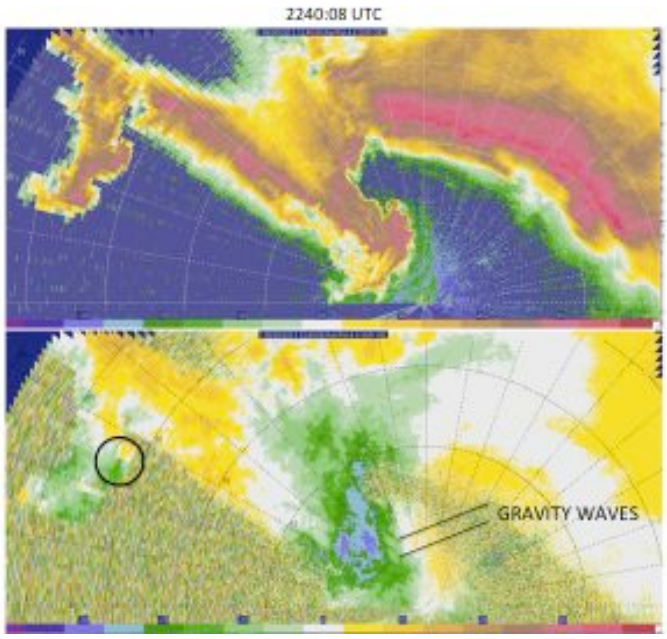

Figure 13: RaXPol data for features shown in Fig. 12, at 4^0 elevation angle, at 2240:08 UTC 30 May 2013; (top) radar reflectivity factor Z (dBZ) and (bottom) Doppler velocity V (m s^{-1}). The hook echo associated with the main storm is accompanied by very weak cyclonic shear, while the funnel cloud to the west is accompanied by strong cyclonic shear (circle).

On 31 May 2013 the genesis of a large, cyclonic tornado and subsidiary vortices, including satellite, multiple sub-vortices and an anticyclonic tornado were documented volumetrically at close range (Figs. 14 – 22). The large tornado and/or one of its multiple vortices were responsible for the deaths of several storm chasers (Wurman et al. 2014). Fig. 14 shows the damage path of the large tornado and two of the most significant deployment sites relative to the damage path. Figs. 15 and 16 show the tornado early on, and multiple-vortices within the large tornado when it was near maturity. Fig. 17 shows polarimetric Doppler data while a separate tornado rotated around the main tornado and was absorbed by it. Fig. 18 shows the tornado during maturity, along with a satellite, sub-vortex. Roger Wakimoto and collaborators are combining

photographs taken from the deployment site with RaXPol data at this time. Figs. 19 and 20 show high-resolution, polarimetric, Doppler-radar data resolving several multiple vortices. Figs. 21 and 22 illustrate the relationship of the anticyclonic tornado to the nearby, large, cyclonic tornado/circulation and the fine-scale structure of the anticyclonic tornado. A polarimetric debris signature was detected in the anticyclonic tornado in both ρ_{hv} and Z_{DR}. Photographic documentation was also obtained (not shown). Kyle Thiem is analyzing data from the El Reno tornado in detail.

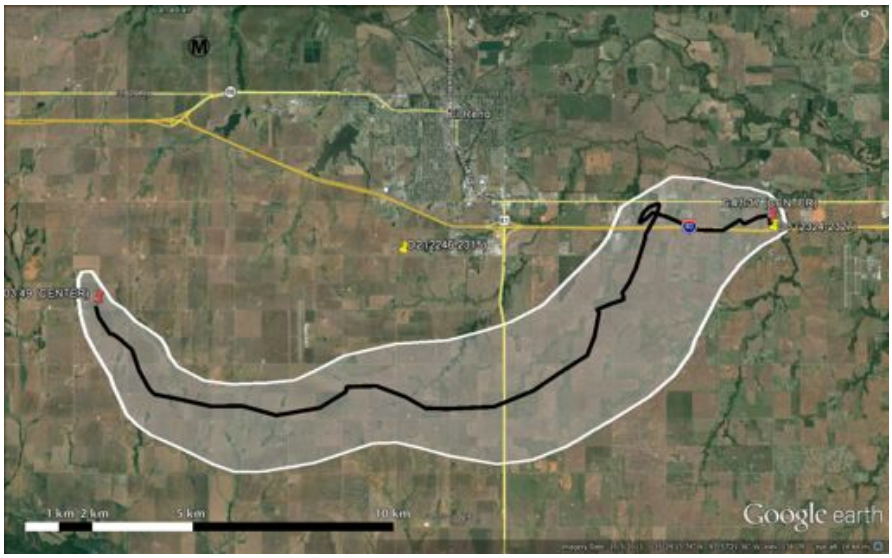

Figure 14: Damage path (white line) and track of TVS (solid black line) for the El Reno, Oklahoma tornado on 31 May 2013. Deployment locations 2 and 3 are indicated by the yellow pins. Times at the deployment sites are given in UTC.

Figure 15: Photograph (© H. Bluestein) looking to the west from deployment site 2 (see Fig. 14) of the early stage of the El Reno tornado.

Figure 16: Photograph (© H. Bluestein) looking to the southwet from deployment site 2 of multiple vortices within the El Reno tornado.

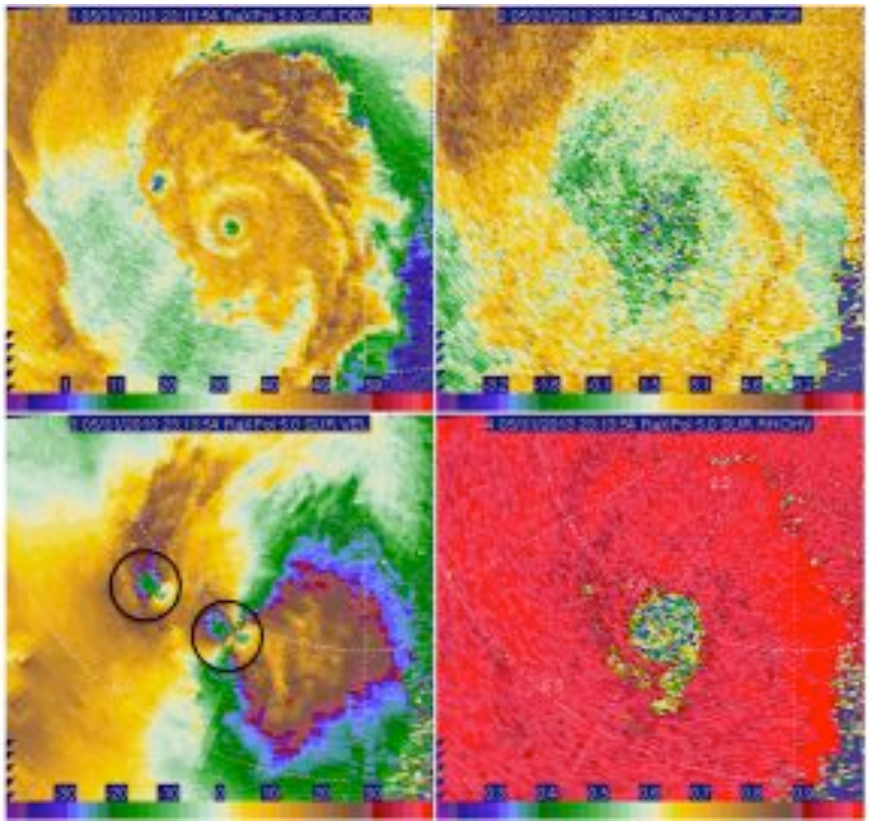

Figure 17: As in Fig. 8, but at deployment site 2 (Fig. 14) at 5^0 elevation angle, at 2313:54 31 May 2013: for two separate tornadoes, each associated with a cyclonic vortex signature (the Doppler velocities have not been de-aliased here) and weak-echo hole (WEH). Range rings shown every 2 km. The tornado to the northwest rotated cyclonically about the main tornado.

Figure 18: Photograph of the El Reno tornado (© H. Bluestein) at deployment site 3 (see Fig. 14), viewed looking to the southwest at 2326 UTC 31 May 2014.

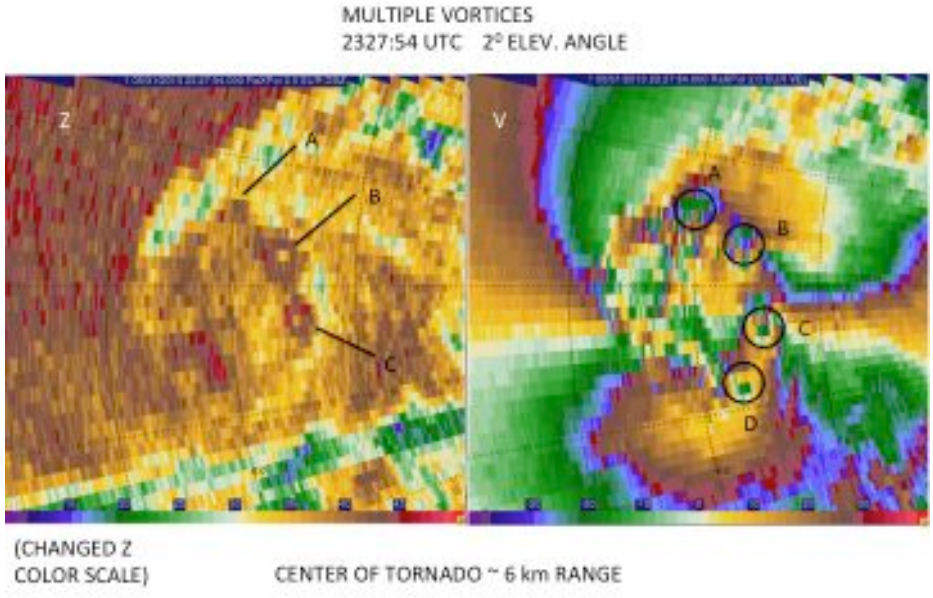

:

Figure 19: Multiple vortices resolved by RaXPol in the El Reno tornado. (left) radar reflectivity Z (dBZ); (right) aliased Doppler velocities V (m s^{-1}). Weak-echo holes (WEH) are labeled A – C, while cyclonic vortex signatures are located with circles and labeled A – D; D is the only one not associated with a WEH. At 2^0 elevation angle at 2327:54 UTC 31 May 2013, at deployment site 3. Range rings plotted every 1 km.

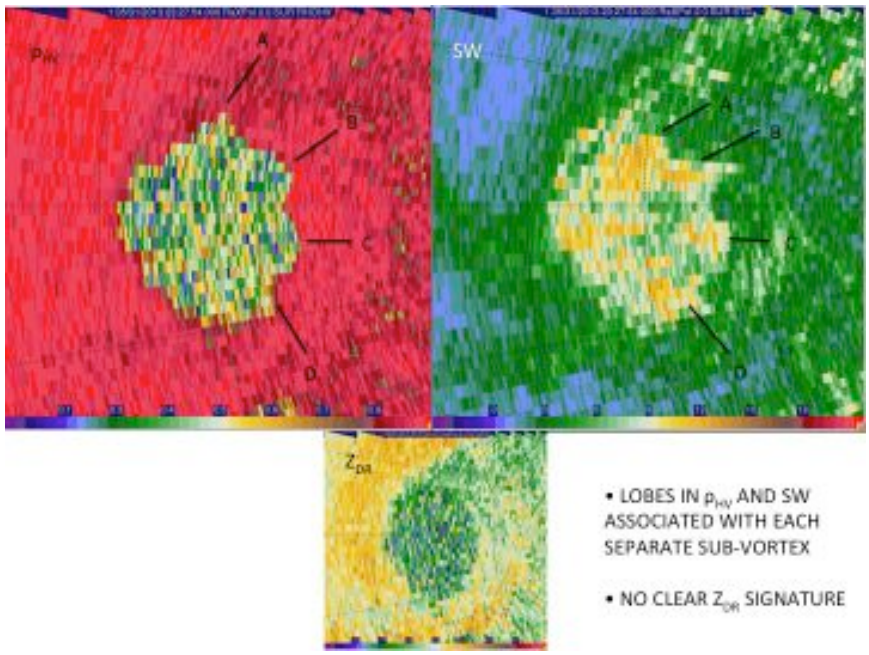

Figure 20: As in Fig. 19, but (top left) co-polar cross-correlation coefficient ρ_{hv}, (top right) spectrum width SW (m s^{-1}), and (bottom) differential reflectivity Z_{DR} (dB).

3 Summary

A number of polarimetric datasets were collected with high spatial resolution with rapid volumetric update times (~ 20 s or less), in which tornadogenesis, tornado evolution, and/or tornado structure were documented. Some of these datasets are now being analyzed. In 2014, volumetric datasets were collected in supercells in Oklahoma, Kansas, Nebraska, and Colorado, but none document tornadogenesis or tornado structure. However, some of these (not shown) are interesting because they document null cases or for other reasons, such as because they document an anticyclonically rotating, left-moving supercell, the evolution of a supercell updraft, the evolution of a multicell line of convection near which a landspout was observed, etc.

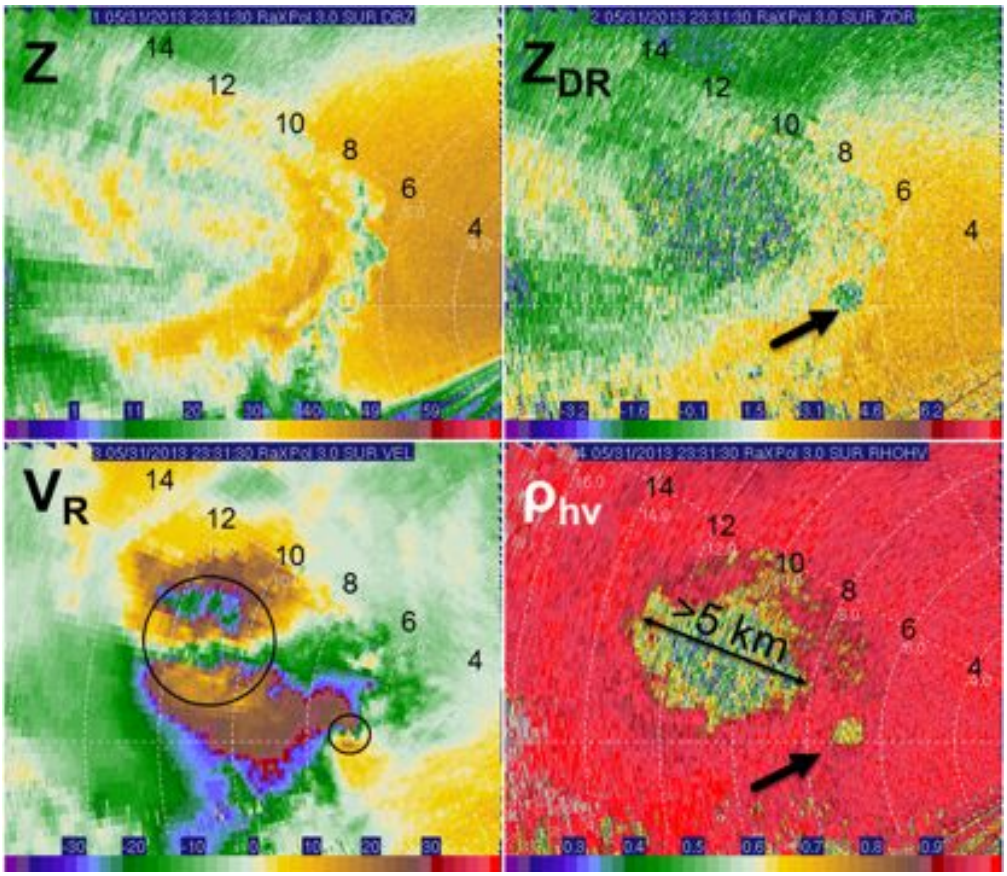

Figure 21: Cyclonic and anticyclonic tornado pair at 2331:30 UTC 31 May 2013, at 3^0 elevation angle, from deployment site 4 (not shown in Fig. 14), to the east southeast of deployment site 3. (upper left) radar reflectivity factor Z (dBZ; (top right) differential reflectivity Z_{DR} (dB); (bottom left) aliased Doppler velocity V (m s^{-1}); (lower right) co-polar cross-correlation coefficient ρ_{hv}. The cyclonic and anticyclonic vortex signatures are circled. The tornado debris signature in ρ_{hv} is over 5 km wide. An arrow points to the debris signature of the anticyclonic tornado.

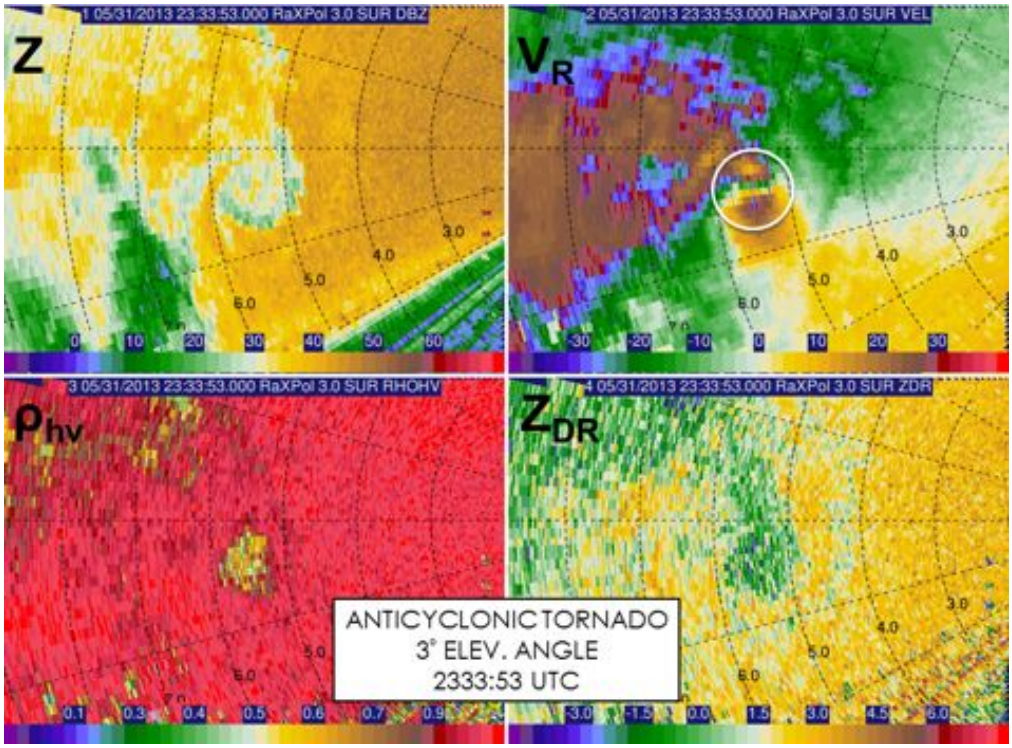

Figure 22: A zoomed-in view of the anticyclonic tornado on 31 May 2013. RaXPol data at 3^0 elevation angle at 2333:53 UTC at deployment site 4 (not shown in Fig. 14). Range rings shown every 1 km. (top left) radar reflectivity factor Z (dBZ); (top right) aliased Doppler velocity V_R (m s^{-1}); (bottom left) co-polar cross-correlation coefficient ρ_{hv}; (bottom right) differential reflectivity Z_{DR} (dB). Doppler wind speeds varied from ~ +30 to – 50 m s^{-1}, i.e., ~ 80 m s^{-1} over ~ 500 m (highlighted by white circle).

Acknowledgments

This work was funded by grants AGS-0934307 and AGS-1262048 from the National Science Foundation. The Advanced Radar Research Center (ARRC) at the University of Oklahoma provided support for maintaining the radar. Some of this extended abstract was prepared while the first author was a visiting scientist at NCAR/MMM during the summer of 2014.

References

Pazmany, A. L., J. B. Mead, H. B. Bluestein, J. C. Snyder, and J. B. Houser, 2013: A mobile, rapid-scanning, X-band, polarimetric (RaXPol) Doppler radar system. *J. Atmos. Ocean. Technol.*, **30**, 1398 – 1413.

Snyder, J. C., and H. B. Bluestein, 2014: Some considerations for the use of high-resolution mobile radar data in tornado intensity determination. *Wea. Foreasting*, **29**, 799 – 827.

Wurman, J., K. Kosiba, P. Robinson, and T. Marshall, 2014: The role of multiple-vortex tornado structure in causing storm researcher fatalities. *Bull. Amer. Meteor. Soc.*, **95**, 31 – 45.